Multielectron processes in close collisions of slow Ne^{q+} ($q=1-9$) ions with Ar atoms

Masamitsu Hoshino,[1,2,*] Tadashi Kambara,[1,†] Yasuyuki Kanai,[1] Reinhold Schuch,[1,3] and Yasunori Yamazaki[1,4]
[1]*Atomic Physics Laboratory, RIKEN, 2-1 Hirosawa, Wako-shi, Saitama 351-0198, Japan*
[2]*Department of Physics, Sophia University, 7-1 Kioicho, Chiyoda-ku, Tokyo 102-8554, Japan*
[3]*Atomic Physics, Stockholm University, S-106 91 Stockholm, Sweden*
[4]*Institute of Physics, University of Tokyo, 3-8-1 Komaba, Meguro-ku, Tokyo 153-8902, Japan*
(Received 1 June 2006; revised manuscript received 1 November 2006; published 28 March 2007)

We have studied the multielectron processes in close collisions between slow Ne^{q+} ions ($q=1-9$, energies of 5 and 14 keV) and Ar atoms through measurements of the charge-state correlations between 27° scattered and 70° recoiling ions. At the selected scattering angle, the internuclear distance of the closest approach at 35 keV is comparable to the *L*-shell radius of Ar atoms. A drastic difference between low-charged ($q=1-3$) and highly charged ($q=7-9$) Ne ions was found. For example, the most probable channel for the Ne^{7+} projectile is three-electron capture accompanied with two-electron loss whereas for the Ne^{+} projectile pure double ionization was found most probable. As a general trend, the mean charges of the both ions and the mean number of captured electrons increase almost linearly with incident charge q, while the mean number of ejected electrons from the system is independent of q at both 5 and 14 keV. We also measured the charge state distributions of the Ar recoil ions as function of the Ne^{q+} ($q=3$, 5, and 7) energies between 5 and 63 keV, which corresponds to distances of closest approach between 0.6 a.u. and 0.17 a.u. We found that the charge of the Ar ions increases at internuclear distances less than 0.32 a.u.

DOI: 10.1103/PhysRevA.75.032722 PACS number(s): 32.80.Hd, 34.20.Mq, 34.70.+e

I. INTRODUCTION

The physics of highly charged ions (HCI's) has become an extremely active field of research since the 1980s. In collisions of slow HCI's with atoms, one of the most important processes is electron capture or charge exchange [1]. Understanding the charge exchange processes plays an important role for basic research as well as a tool in a large number of fields—e.g., astrophysics, fusion plasma diagnostics, and interactions of ions with solids. In the interaction of slow HCI's with metal surfaces it is known that the approaching ions capture electrons from the surface into highly excited states and form hollow atoms at rather large distances from the surface, especially in grazing collisions [2]. Hollow atoms outside of the surface have also been studied with beam-capillary spectroscopy where x rays and visible photons were observed from HCI's which passed through a microcapillary target [3–5]. On the other hand, collision processes in large-angle scattering of slow HCI's from surfaces are different from the grazing collisions. In the former, the ions are scattered by a binary hard collisions with an atom on the surface whereas in the latter the ion experiences successive soft collisions. Recently, studies [6–13] have been reported on the neutralization processes in large-angle scattering of slow, highly charged Ar ions on Au surfaces. The neutralization processes have been explained by model calculations, which included the processes of electron capture, recapture, and Auger transitions assuming single binary ion-atom collisions. These models neglect, however, completely ionization and electron emission during scattering. It has been questioned whether this assumption is justified. For a clarification it is important to study these processes under well-defined conditions. We have thus investigated close and single collisions of slow HCI's with single atoms, as an elementary processes of the ion-surface interactions.

Several studies on inner-shell excitations in close collisions of low-charged ions with atoms were done in the 1950s and 1960s [14]. Angular differential cross sections were measured for scattered-ion charge states at 25–100 keV [15,16], and the results were used to determine the potential energy functions for several collision systems [17]. All these experiments were done for singly charged ions, where the ionization channels dominate. Also, charge-state correlations between scattered and recoil ions were measured with a coincidence technique in large-angle scattering of Ar^{+} on Ar [18,19] and for Ne, Ne^{+}, and Ne^{2+} on Ne [20,21] in a few hundred keV region. They have led to a model of electron promotion on quasimolecular orbitals [22,23]. All experiments were done for low-charged ions at relatively high impact energies, where the ionization dominates over the electron capture channels. This can be different from highly charged incoming ions. In that case, it is unclear how many electrons will be transferred to the highly charged projectile, whether the charge is equilibrated in a close collision, and how strong the ionization channel still is.

Concerning collisions of HCI's with atoms, only a few measurements of the charge-state correlation between scattered and recoil ions have been reported at relatively small scattering angles. The charge-state correlation in collisions of 90-keV Ne^{7+} ions with Ne at angles up to 1.2° and of 90-keV Ne^{9+} ions with Ne up to 4.3° was measured by Schmidt-Böcking *et al.* [24] and Herrmann *et al.* [25], respectively. In these measurements with HCI's, the multielectron transfer is found to be the dominant channel, in contrast to the early measurements with singly charged ions, where the direct ionization channels were found to be important [18,19]. There

*Electronic address: masami-h@sophia.ac.jp
†Present address: Accelerator Applications Research Group, RIKEN Nishina Center.

 ©2007 The American Physical Society

has not been any systematic measurements of projectile charge-state dependence for close and single collisions between slow highly charged ions and atomic targets.

In this paper, we present systematic studies of electronic processes in close encounters of slow highly charged Ne ions with Ar atoms, at various charge states (q) and energies (E) of the projectile. Two kinds of measurements are reported: first, the charge-state correlations of scattered and recoil ions in close collisions between slow Ne^{q+} ($q=1-9$, $E=5$ and 14 keV, velocities $v=0.10$ and 0.17 a.u.) ions and Ar atoms. This corresponds to the measurement of the incident charge state dependence at fixed distance of closest approach. We have reported a part of these measurements at lower incident charge states ($q=1$, 2, and 3) at 5 keV in Ref. [26]. Second, we did measurements of recoil-ion charge-state distributions for Ne^{q+} ($q=3$, 5, and 7) impacts as a function of the impact energy between 5 and 63 keV, which corresponds to $v=0.10-0.35$ a.u. This measurement should reveal the distance of closest approach dependence at fixed incident charge state. The scattering angle was in all cases fixed at $\Theta_{c.m.}=40°$ in the center-of-mass system. The corresponding distance of closest approach is estimated to be between 0.60 a.u. at 5 keV and 0.17 a.u. at 63 keV. Since the $2p$-orbit radius of Ar is about 0.29 a.u. and that of Ne is about 0.6 a.u. [27], the atomic L shells of the collision partners interpenetrate each other in the present conditions. The distances are by an order of magnitude smaller than for the first electron transfer from the classical overbarrier (COB) model, which were calculated to be about 6.6 a.u. for Ne^{+}-Ar and 27.5 a.u. for Ne^{7+}-Ar [28].

II. EXPERIMENTS

The experiments were carried out at the Slow Highly Charged Ion Beam Facility in RIKEN [29]. A Ne-ion beam extracted from a Caprice-type ECR ion source was analyzed by a dipole magnet to a desired energy and charge state between 1+ and 9+. Then the beam was focused by a magnetic quadrupole triplet lens and guided to a vacuum chamber with a diameter of 50 cm.

Figure 1 shows a schematic view of the detection system inside the chamber. The beam was collimated by a rectangular aperture with 2 mm in width and 4 mm in height and transmitted through a differentially pumped collision region with a diameter of 22 mm at the center of the vacuum chamber. The target Ar gas was introduced through a needle at right angle to the beam direction. The pressure in the vacuum chamber was about 1.3×10^{-4} Pa. The single-collision conditions for electron transfer were confirmed at this target-gas pressure by measurements of recoil-ion yield as a function of the pressure. The base pressure without the target gas was about 1.3×10^{-5} Pa. The scattered Ne ions and recoil Ar ions from the collision region were detected by ion-detection telescopes with an acceptance angle of ±5° at angles of $\theta_{Ne}=27°$ and $\theta_{Ar}=70°$ in the laboratory system, respectively. This angle combination fulfills the kinematics relation of elastic scattering for the Ne-Ar collision system. Each detection telescope consisted of a time-of-flight (TOF) drift tube and a two-dimensional position-sensitive detector (2D-PSD),

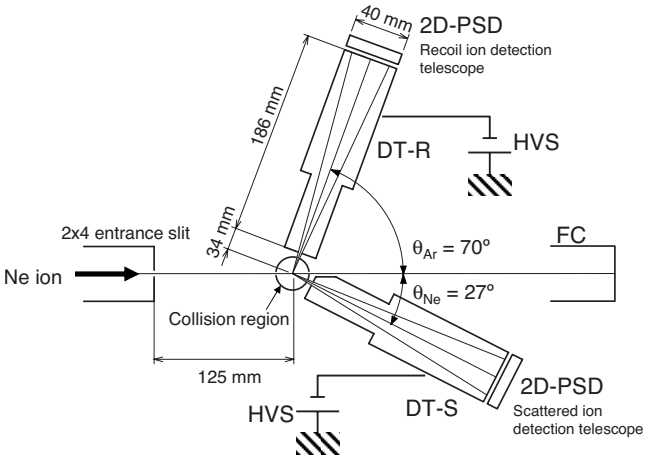

FIG. 1. A schematic view of the detection system in a collision chamber. 2D-PSD means two-dimensional position-sensitive detector, and DT-S and DT-R are time-of-flight drift tubes for scattered and recoil ions. HVS is the high-voltage power supply to bias the drift tubes, and FC is the Faraday cup.

which had microchannel plates (MCP) with a diameter of 40 mm and a wedge-and-strip anode [30]. The drift tubes are named DT-S and DT-R for the scattered and recoil ions respectively as shown in Fig. 1. The DT-S and DT-R can independently be biased electrostatically. The voltage of the DT-S is expressed hereafter as $V_{DT\text{-}S}$ and that of DT-R as $V_{DT\text{-}R}$. The biased drift tube modulates the velocity, and thus the TOF, of the outgoing ions according to their charge states. The TOF difference between the scattered Ne and recoil Ar ions ($\Delta\mathcal{T}$) was measured with a time-to-amplitude converter (TAC) started by a fast signal from the scattered-ion detector and stopped by one from the recoil-ion detector. The kinematical condition eliminates almost completely coincident scattering events from residual gas and from the tip of the gas-injection needle.

According to the kinematics of elastic scattering, the TOF of the scattered and recoil ions depend considerably on the detection angles within the acceptance angle of the detection telescope and the measurement of the $\Delta\mathcal{T}$ only is not sufficient to identify the charge states of the ions. Therefore, for each coincidence event, we recorded in a list mode not only the $\Delta\mathcal{T}$ but also the positions of both ions on the 2D-PSD. The combination of the charge states of the scattered and recoil ions (q_{Ne}, q_{Ar}) was determined from the ion positions and $\Delta\mathcal{T}$, as described in the following paragraphs. The relation between the energy and TOF of scattered and recoil ions at 5, 14, and 50 keV and $\theta_{Ne}=27°$ is shown in Table I, where E_0, E_{Ne}, $\mathcal{T}_{Ne}$, E_{Ar}, and $\mathcal{T}_{Ar}$ show the incident energy, kinetic energy and flight time of scattered Ne ions, kinetic energy, and flight time of recoil Ar ions, respectively.

The position on the detector was calibrated by using an α source and a mask with holes. Since we observed a distortion near the edge of the MCP, we analyzed only the events in which ions hit a certain area on the detector where the position linearity was confirmed within 0.25°. This area covers an acceptance angle of ±4°.

In order to identify q_{Ne} and q_{Ar} from the ion positions and $\Delta\mathcal{T}$, the measurements were performed in three steps. This

TABLE I. The relation between energy and TOF of scattered and recoil ions at 5, 14, and 50 keV and $\theta_{Ne}=27°$.

E_0 (keV)	E_{Ne} (keV)	$\mathcal{T}_{Ne}$ (μsec)	E_{Ar} (keV)	$\mathcal{T}_{Ar}$ (μsec)	$\Delta\mathcal{T}$ (μsec)
5	4.477	1.062	0.523	4.396	3.334
14	12.536	0.635	1.464	2.627	1.992
50	44.771	0.336	5.229	1.390	0.718

procedure is demonstrated in Fig. 2 for the case of 5-keV Ne^+ impact. In the first step, we grounded the DT-S and DT-R ($V_{DT\text{-}R}=V_{DT\text{-}S}=0$) and measured the two-dimensional distribution of $\Delta\mathcal{T}$ versus θ_{Ne}. In this case, since the ion velocity is independent of the charge state, the coincidence events are scattered along one line determined by the elastic-scattering kinematics, shown as a ridge in Fig. 2(a). This relation between $\Delta\mathcal{T}$ and θ_{Ne} gives the reference position to identify q_{Ar} in the next step, where only $V_{DT\text{-}R}$ was set to -1.8 kV for modulating the recoil-ion velocity. Consequently, the ridge in Fig. 2(a) separates into several ridges according to q_{Ar} as shown in Fig. 2(b). Finally, we set both $V_{DT\text{-}S}$ and $V_{DT\text{-}R}$ to -1.8 kV. Then each of the ridges of a q_{Ar} separates into multiple ridges corresponding to different q_{Ne}, as shown in Fig. 2(c). The separation between the recoil-ion ridges is larger than that for the scattered ions, because the velocity of recoil ions is much lower than that of the scattered ions.

Since the ridges in Fig. 2(c) are almost parallel to each other, a linear transformation of $\Delta\mathcal{T}$ and scattering angle θ_{Ne}, $\Delta\mathcal{T}^*=\Delta\mathcal{T}+a\theta_{Ne}$, was employed with a coefficient a adjusted so that the ridges on the $\Delta\mathcal{T}^*$-θ_{Ne} plane were perpendicular to the $\Delta\mathcal{T}^*$ axis. Then, the two-dimensional plot was projected onto the $\Delta\mathcal{T}^*$ axis. The results were corrected for the efficiency of the MCP given by Krems *et al.* [31] which was about 0.42 at lowest for the recoil Ar^+ ions from 5-keV Ne projectile, and increased for higher energy and charge states up to an asymptotic value of 0.58.

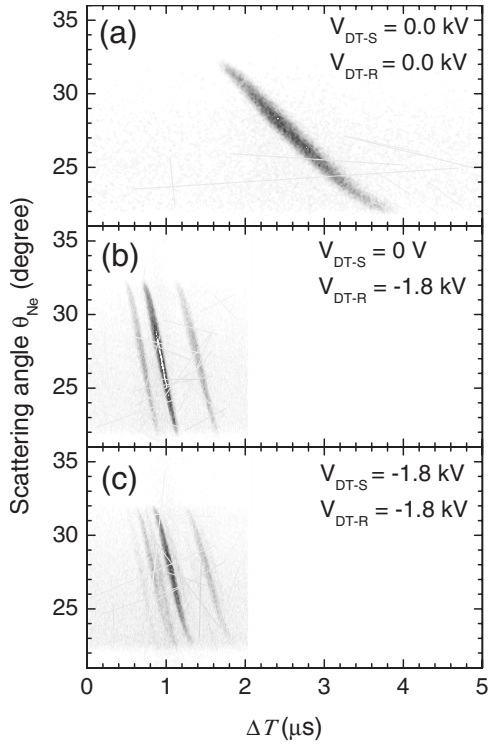

FIG. 2. Two-dimensional plots of coincidence events for $\Delta\mathcal{T}$ and scattering angle in collisions of 5-keV Ne^+ ions with Ar atom.

III. RESULTS

A. Charge-state correlations

Figure 3 shows the $\Delta\mathcal{T}^*$ spectra measured with 5-keV Ne^{q+}: (a) for $q=1$ and (b) for $q=7$. The upper spectra in Fig. 3 were taken with the $V_{DT\text{-}R}=-1.8$ kV and $V_{DT\text{-}S}=0$, while $V_{DT\text{-}R}=V_{DT\text{-}S}=-1.8$ kV was set for the lower spectra. In the upper spectrum in Fig. 3(a), there are three peaks which are separated according to the charge states of the Ar recoil ions, q_{Ar}. In the lower spectrum, each of the peaks shifts to larger $\Delta\mathcal{T}^*$ values and splits into multiple peaks according to the charge states of the scattered ions, q_{Ne}. The charge states q_{Ar} and q_{Ne} shown in the spectra were assigned from a calculation of the TOF in the drift tubes. Before, we reported in detail the charge-state distribution of the scattered and recoil ions for Ne^{q+} ($q=1$, 2, and 3) on Ar at 5 keV [26].

In the lower spectrum of Fig. 3(b), the expected $\Delta\mathcal{T}^*$ peak positions are shown for different values of q_{Ne}. It is seen that the combination of charge states (q_{Ne}, q_{Ar}) distributes in $2<q_{Ne}<6$ and $2<q_{Ar}<8$ for the Ne^{7+} projectile. The average charge state of the scattered ion $\langle q_{Ne}\rangle$ was estimated to be 4.3 and of the recoil ion $\langle q_{Ar}\rangle$ was 5.0; i.e., three-electron capture accompanied by two-electron ionization is the most probable channel. With a similar analysis for the 5-keV Ne^{4+} ion case, the $\langle q_{Ne}\rangle$ and $\langle q_{Ar}\rangle$ were estimated to be 2.4 and 3.5, respectively, and the corresponding most probable channels are found to be two-electron capture accompanied by two-electron ionization. As we reported previously [26], the most probable channel for 5-keV Ne^+ ion was found to be $q_{Ne}=1$ and $q_{Ar}=2$ which corresponds to pure two-electron ionization which is very different from the highly charged Ne cases.

From the experimental results of the charge-state correlation of recoil and scattered ions, we obtained the average charges of scattered ions, $\langle q_{Ne}\rangle$, and recoil ions, $\langle q_{Ar}\rangle$, for Ne^{q+} ($q=1-9$) on Ar atoms. We also deduced the number of electrons ejected from the collision systems, $\langle n_e\rangle=\langle q_{Ne}\rangle+\langle q_{Ar}\rangle-q$, and the number of electrons captured by the projectile, $\langle n_c\rangle=q-\langle q_{Ne}\rangle$. Figures 4(a)–4(c) show the results for $\langle q_{Ne}\rangle$, $\langle q_{Ar}\rangle$, $\langle n_e\rangle$, and $\langle n_c\rangle$ as functions of the incident charge state q, respectively. The variation of $\langle q_{Ar}\rangle$ by the MCP efficiency correction is about 3% at 5 keV and 1.5% at 14 keV, which is within the indicated error bars. The values of $\langle q_{Ne}\rangle$ and $\langle q_{Ar}\rangle$ increase almost linearly with q and the rate of increase per incident charge is similar between the impact energies of 5 and 14 keV. As a result, $\langle n_c\rangle$ also increases almost linearly from zero at $q=1$ to 3 at $q=9$, while $\langle n_e\rangle$ stays between 2 and 3 and is nearly independent of q at both impact energies. Therefore, under the present collision con-

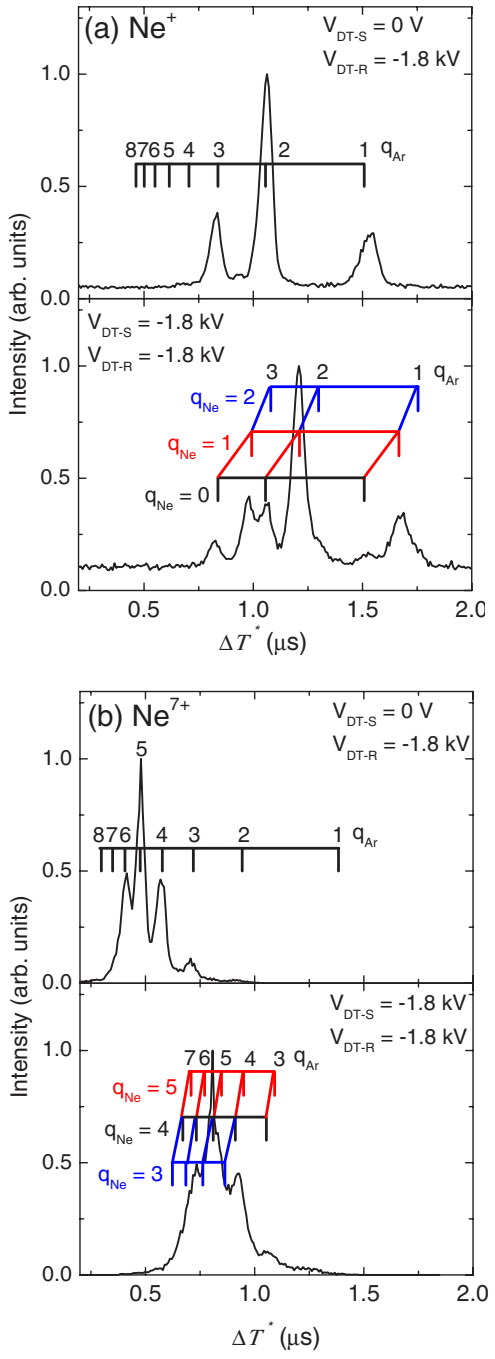

FIG. 3. (Color online) The spectra of ΔT^* between scattered Ne and recoil Ar ions measured for (a) Ne^+ and (b) Ne^{7+} ions at 5 keV on Ar, obtained by projecting the two-dimensional maps of ΔT vs scattering angle θ_{Ne}. Upper spectra: $V_{DT\text{-}R}=-1.8$ kV and $V_{DT\text{-}S}=0$ where the numbers corresponded to q_{Ar}. Lower spectra: $V_{DT\text{-}R}=V_{DT\text{-}S}=-1.8$ kV, and the numbers correspond to combinations of q_{Ar} and q_{Ne}.

ditions, the most probable channel is pure two-electron ionization from Ar for $q=1$ and single- to multiple-electron capture accompanying a two-electron ionization for higher q. This holds for both the impact energies of 5 and 14 keV.

In addition to the general trend mentioned above, Fig. 4(b) shows a slight increase of $\langle q_{Ar}\rangle$ with incident energy at small incident charge states $q \leqslant 3$. A similar increase of $\langle n_e\rangle$

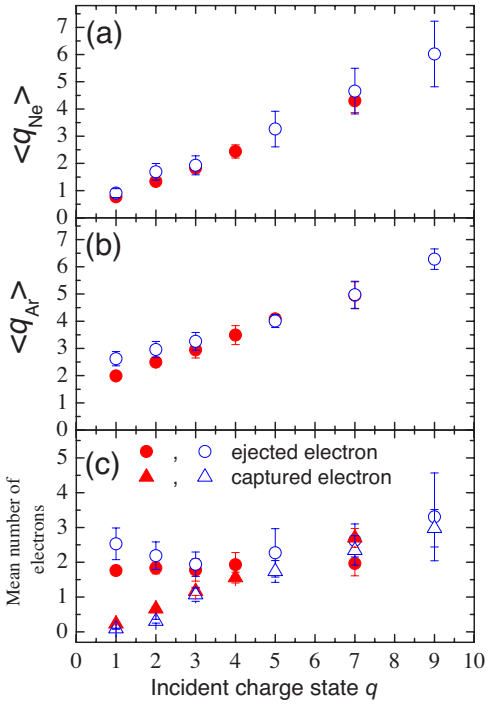

FIG. 4. (Color online) The mean charge states of (a) scattered ions $\langle q_{Ne}\rangle$, (b) recoil ions $\langle q_{Ar}\rangle$, and (c) the mean number of electrons ejected from the system $\langle n_e\rangle$ $[=\langle q_{Ne}\rangle+\langle q_{Ar}\rangle-q]$ and captured electrons by the projectile, $\langle n_c\rangle$ $(=q-\langle q_{Ne}\rangle)$, as functions of incident charge q. Solid and open symbols correspond to the projectile energy of 5 keV and 14 keV, respectively.

is observed in Fig. 4(c); however, $\langle q_{Ne}\rangle$ in Fig. 4(a) does not show such behavior. The increase of $\langle n_e\rangle$ is due to the enhancement of the target ionization revealed by the shifts of q_{Ar} distributions in Fig. 5.

B. Recoil-ion charge-state distributions

From the ΔT^* spectra with DT-R biased only, we obtained the q_{Ar} distributions for incident charge states $q=1$, 2, 3, 5, and 7. Figures 5(a) and 5(b) show the results at 14 keV and 5 keV, respectively. The distribution shifts to higher q_{Ar} with increasing q for both incident energies of 5 and 14 keV. The q_{Ar} distributions for Ne^{5+} and Ne^{7+} impact were almost the same for 5 and 14 keV. However, for the lower incident charge states, $q=1-3$, the distribution shifts slightly to higher q_{Ar} at the higher projectile energy.

To study the general behavior of the target ionization in a wider incident-energy range, the recoil-ion charge state q_{Ar} distributions have been measured for Ne^{q+} ($q=3$, 5, and 7) impact, with the same setup and $V_{DT\text{-}R}=-1.8$ kV at $E=5-63$ keV. This corresponds to a measurement of the distance of closest-approach dependence of the recoil charge states at fixed incident charge state. This is expected to give more insights in the relative importance of target ionization and electron capture.

Figure 6 shows the $\langle q_{Ar}\rangle$ for the impact of Ne^{3+}, Ne^{5+}, and Ne^{7+} as a function of the internuclear distance of closest approach (R_N) which has been estimated from the deflection

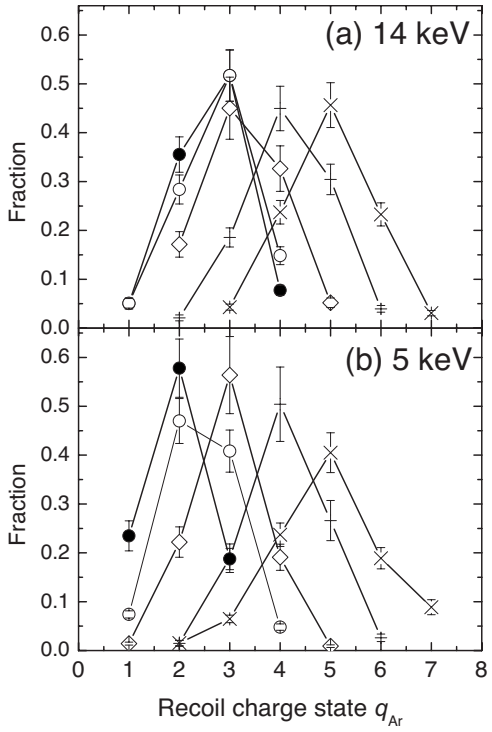

FIG. 5. Charge-state distributions of recoil ions in collisions of Ne^{q+} (q=1, 2, 3, 5, and 7) with Ar at (a) 14 keV and (b) 5 keV. (●) q=1, (○) q=2, (◇) q=3 (+) q=5, and (×) q=7.

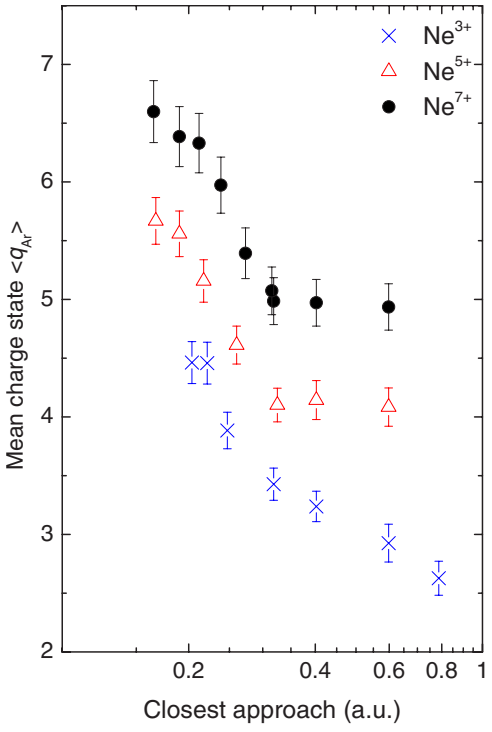

FIG. 6. (Color online) The mean charge state of recoil ions plotted as a function of the closest approach in collisions of Ne^{q+} with Ar where (×) for q=3, (△) for q=5, and (●) for q=7.

function of classical trajectory in a screened Coulomb potential [32],

$$V(r) = (Z_1 Z_2 e^2/r)\exp(-r/a),$$

where Z_1=10 and Z_2=18 is the projectile and target atomic number, respectively, and a common value of the screening parameter $a=a_0/(Z_1^{2/3}+Z_2^{2/3})^{1/2}$ with Bohr radius a_0 is adopted for all incident charges.

As shown by Fig. 6, the behavior of $\langle q_{Ar}\rangle$ changes at a certain R_N with decreasing R_N or increasing the impact energy. For q=5 and 7, $\langle q_{Ar}\rangle$ steeply increases below R_N =0.3 a.u., while it is almost constant at larger R_N. For q=3, $\langle q_{Ar}\rangle$ increases continuously with decreasing R_N but the slope becomes steeper at R_N=0.3 a.u. The critical R_N is independent of q and corresponds to the 2p-orbit radius of Ar atom which is estimated as 0.29 a.u. Opening the 2s shell for q=7 does not seem to have a strong influence on $\langle q_{Ar}\rangle$.

C. Discussion

The incident-charge (q) dependence of the charge-state correlation presented in Sec. III A shows a relatively simple feature both at 5 and 14 keV. The number of captured electrons, n_c, linearly increases with q while that of the ejected electron, n_e, stays almost constant between 2 and 3, with a possible exception for q=9 where n_e seems to increase.

These findings are compared with experiments at distant collisions where final states were analyzed by recoil-ion momentum spectroscopy (RIMS) [33]. Zhang *et al.* [34] studied final-state distributions in single- and multiple-electron capture processes in 105-keV N^{7+} on Ar. They found that the most probable channel was single-electron capture. Multiple-electron capture populates multiply excited states of the scattered ions which most likely autoionize. For example, two-electron autoionization was found [34] most probable in quadruple-electron capture while no electrons were ejected in single-electron capture. Thus the number of ejected electrons increased with that of captured electrons. This is different in our findings. The electron emission in our case is not dominantly from autoionization after electron capture, but rather target ionization during the collision.

In order to discuss the ionization process, we apply the molecular-orbital (MO) model to the Ne^{q+}-Ar system. Figure 7 shows the energies of the adiabatic MO's for a neutral Ne-Ar system calculated with the DV-$X\alpha$ method explained in Ref. [35] as functions of the internuclear distance. This is consistent with the correlation diagram given by Larkins [36]. Due to a diabatic crossing at about 0.2–0.3 a.u., radial coupling can cause transitions among the 4σ, 5σ, and 6σ channels since these MO's cross in a diabatic correlation diagram, as stated in Refs. [36,37]. At smaller internuclear distances, an incoming Ne L-shell vacancy can be transferred to the L shell of Ar. The subsequent Auger process ionizes the recoil Ar ion; i.e., electrons in the L shell of Ar are captured in close collisions by highly charged Ne ions and two vacancies in Ar are created by this process. In Fig. 6 an increase of $\langle q_{Ar}\rangle$ by almost two charges is seen. Therefore, we attribute the increase of the recoil-ion charge to this Auger ionization after electron capture by the highly charged Ne ions.

At an internuclear distance larger than 0.3 a.u., the correlation diagram has no crossings which can promote the Ar L

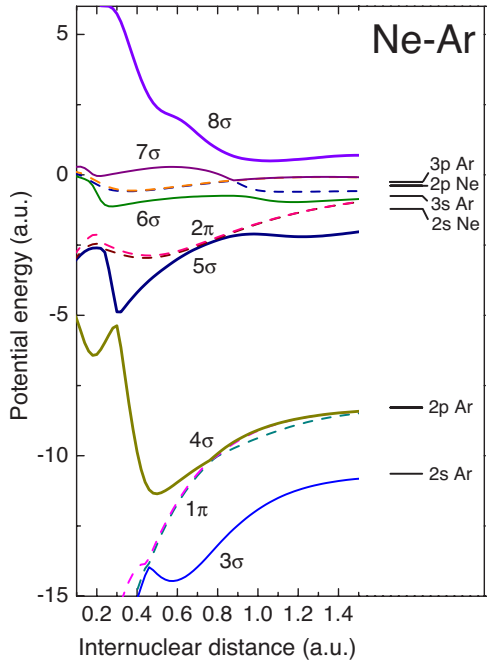

FIG. 7. (Color online) Correlation diagram calculated by DV-$X\alpha$ method [35]. Solid curves: σ channels. Dashed curves: π channels.

electrons to higher shells. Therefore, the Auger effect, following electron promotion, seems not to be important for ionization. From these data we conclude that even in these slow ion collisions electrons are ejected during the collision, i.e., at the closest approach, rather than by Auger processes after the collision. In the correlation diagram, the 8σ MO is promoted at an internuclear distance of 0.6 a.u. which may cause the ionization of Ar $3p$ electrons. It may explain the observed target ionization at 5 and 14 keV.

As presented in Sec. III B and seen in Fig. 6, the charge of the recoil ions from Ne^{3+} impact increases slowly at decreasing internuclear distance. This is also shown in Fig. 5 where the recoil-ion charge distribution shifts to higher values for the impact of Ne^{q+} ($q=1-3$) when the projectile energy increases from 5 to 14 keV, while the mean charge of the scattered Ne ions stays unchanged with the projectile energy as shown in Fig. 4. Thus, at lower-charge states ($q \leqslant 3$) the direct target ionization, which is there the dominant channel to produce the recoil ions, increases with the projectile energy. At higher-charge-state impacts ($q=5$ and 7), on the other hand, the recoil charge state is almost constant above an internuclear distance of 0.3 a.u. Thus the capture channels are indeed very important at higher projectile charge states and their contribution has a weak dependence on the internuclear distances studied here.

IV. CONCLUSION

The charge-state correlations of scattered ions and recoil ions in close collisions of slow Ne^{q+} ($q=1-9$) ions with Ar atoms have been measured. We found that the mean charge of the ion pairs and number of captured electrons increases almost linearly with the incident charge q, while the number of ejected electrons from the collision system is independent of q at both 5 and 14 keV.

Thus direct ionization seems to be independent of the charge, and for high-charge states electron capture becomes important, but autoionization of the captured excited states does not seem to contribute much. This is partly in contradiction to results at small scattering angles by other groups.

By varying the collision energy, the distance of closest approach for Ne^{3+}, Ne^{5+}, and Ne^{7+} impact could be changed between 0.17 and 0.60 a.u. In that range (at about 0.3 a.u., corresponding to the L-shell radius of Ar) a steplike increase of the mean charges of the recoil ions was found. Partly, these results are qualitatively explained by electron promotion from Ar $2p$ using a calculated molecular orbital diagram. We thus observe a clear shell effect at the L-shell radius of Ar, which is almost the same effect as assumed in simulations of ion-surface interactions. Otherwise, we notice a clear difference between slow collisions with isolated atoms and solid surfaces as a target: Even in close ion-atom collisions, we do not find an indication of hollow atom formation and also neutralization is not observed like in collisions with solid surfaces. We confirm, however, that direct ionization is an important channel for electron emission.

ACKNOWLEDGMENTS

M.H. has been supported by Special Postdoctoral Researchers Program at RIKEN. R.S. acknowledges the RIKEN eminent scientist program for the support during his stay at RIKEN. The authors are grateful to K. Senoo and other members of the Research Instruments Development Division of RIKEN for the design and construction of the gas target and the ion-detection telescopes and to Dr. K. Ohtsuki of The University of Electro-Communications for useful discussions.

[1] R. K. Janev and H. Winter, Phys. Rep. **117**, 265 (1985) and references therein.
[2] H. Winter, C. Auth, R. Schuch, and E. Beebe, Phys. Rev. Lett. **71**, 1939 (1993).
[3] Y. Yamazaki, S. Ninomiya, F. Koike, H. Masuda, T. Azuma, K. Komaki, K. Kuroki, and M. Sekiguchi, J. Phys. Soc. Jpn. **65**, 1199 (1996).
[4] S. Ninomiya, Y. Yamazaki, F. Koike, H. Masuda, T. Azuma, K. Komaki, K. Kuroki, and M. Sekiguchi, Phys. Rev. Lett. **78**, 4557 (1997).
[5] Y. Morishita, R. Hutton, H. A. Torii, K. Komaki, T. Brage, K. Ando, K. Ishii, Y. Kanai, H. Masuda, M. Sekiguchi, F. B. Rosmej, and Y. Yamazaki, Phys. Rev. A **70**, 012902 (2004).
[6] W. Huang, H. Lebius, R. Schuch, M. Grether, and N. Stolterfoht, Phys. Rev. A **58**, 2962 (1998).
[7] W. Huang, H. Lebius, R. Schuch, M. Grether, A. Spieler, and

N. Stolterfoht, Nucl. Instrum. Methods Phys. Res. B **135**, 336 (1998).
[8] R. Schuch, W. Huang, H. Lebius, Z. Pešić, N. Stolterfoht, and G. Vikor, Nucl. Instrum. Methods Phys. Res. B **157**, 309 (1999).
[9] Z. D. Pešić, H. Lebius, R. Schuch, Gy. Vikor, V. Hoffman, D. Niemann, and N. Stolterfoht, Nucl. Instrum. Methods Phys. Res. B **164–165**, 511 (2000).
[10] F. W. Meyer, V. A. Morozov, S. Datz, and R. Vane, Phys. Scr. **T92**, 182 (2001).
[11] V. A. Morozov and F. W. Meyer, Phys. Rev. Lett. **86**, 736 (2001).
[12] Z. D. Pešić, J. Anton, J. H. Bremer, V. Hoffman, N. Stolterfoht, Gy. Vikor, and R. Schuch, Nucl. Instrum. Methods Phys. Res. B **203**, 96 (2003).
[13] F. W. Meyer, H. F. Krause, V. A. Morozov, C. R. Vane, and L. I. Vergara, Phys. Scr. **T110**, 403 (2004).
[14] J. D. Garcia, R. J. Fortner, and T. M. Kavanagh, Rev. Mod. Phys. **45**, 111 (1973).
[15] E. N. Fuls, P. R. Jones, F. P. Ziemba, and E. Everhart, Phys. Rev. **107**, 704 (1957).
[16] F. P. Ziemba, G. J. Lockwood, G. H. Morgan, and E. Everhart, Phys. Rev. **118**, 1552 (1960).
[17] G. H. Lane and E. Everhart, Phys. Rev. **120**, 2064 (1960).
[18] G. H. Morgan and E. Everhart, Phys. Rev. **128**, 667 (1962).
[19] E. Everhart and Q. C. Kessel, Phys. Rev. Lett. **14**, 247 (1965).
[20] Q. C. Kessel, M. P. McCaughey, and E. Everhart, Phys. Rev. Lett. **16**, 1189 (1966).
[21] M. P. McCaughey, E. J. Knystautas, H. C. Hayden, and E. Everhart, Phys. Rev. Lett. **21**, 65 (1968).
[22] U. Fano and W. Lichten, Phys. Rev. Lett. **14**, 627 (1965).
[23] W. Lichten, Phys. Rev. **164**, 131 (1967).
[24] H. Schmidt-Böcking, M. H. Prior, R. Dörner, H. Berg, J. O. K. Pedersen, C. L. Cocke, M. Stockli, and A. S. Schlachter, Phys. Rev. A **37**, 4640 (1988).
[25] R. Herrmann, M. H. Prior, R. Dörner, H. Schmidt-Böcking, C. M. Lyneis, and U. Wille, Phys. Rev. A **46**, 5631 (1992).
[26] M. Hoshino, T. Kambara, Y. Kanai, R. Schuch, and Y. Yamazaki, Nucl. Instrum. Methods Phys. Res. B **235**, 347 (2005).
[27] J. C. Slater, *Quantum Theory of Atomic Structure* (McGraw-Hill, New York, 1960).
[28] A. Niehaus, J. Phys. B **19**, 2925 (1986).
[29] Y. Kanai, D. Dumitriu, Y. Iwai, T. Kambara, T. M. Kojima, A. Mohri, Y. Morishita, Y. Nakai, H. Oyama, N. Oshima and Y. Yamazaki, Phys. Scr. **T92**, 467 (2001).
[30] C. Martine, P. Jelinsky, M. Lampton, R. F. Malina, and H. O. Anger, Rev. Sci. Instrum. **52**, 1067 (1981).
[31] M. Krems, J. Zirbel, M. Thomason, and R. D. DuBois, Rev. Sci. Instrum. **76**, 093305 (2005).
[32] E. Everhart, G. Stone, and R. J. Carbone, Phys. Rev. **99**, 1287 (1955).
[33] R. Dörner, V. Mergel, O. Jagutzki, L. Spielberger, J. Ullrich, R. Moshammer, and H. Schmidt-Böcking, Phys. Rep. **330**, 95 (2000).
[34] H. Zhang, X. Fléchard, A. Cassimi, L. Adoui, G. Cremer, F. Frémont, and D. Hennecart, Phys. Rev. A **64**, 012715 (2001).
[35] H. Adachi, M. Tsukada, and C. Satoko, J. Phys. Soc. Jpn. **45**, 875 (1978).
[36] F. P. Larkins, J. Phys. B **5**, 571 (1972).
[37] R. Soda, K. Yamamoto, W. Hayami, T. Aizawa, and Y. Ishizawa, Surf. Sci. **343**, 104 (1995).